

Probing unexplored spin-dependent dark matter-proton coupling with few-photoelectron threshold in COSINE-100

W. K. Kim,^{1,2,*} N. Carlin,³ J. Y. Cho,⁴ S. J. Cho,² S. Choi,⁵ A. C. Ezeribe,⁶ L. E. França,³ R. F. Muhdi,⁷ O. Gileva,² C. Ha,⁸ I. S. Hahn,^{9,10,1} E. J. Jeon,^{2,1} H. W. Joo,⁵ W. G. Kang,² M. Kauer,¹¹ B. H. Kim,² D. Y. Kim,² H. J. Kim,⁴ J. Kim,⁸ K. W. Kim,² S. H. Kim,² S. K. Kim,⁵ Y. D. Kim,^{2,1} Y. H. Kim,^{2,1} B. R. Ko,¹² Y. J. Ko,^{13,†} B. C. Koh,⁸ D. H. Lee,⁴ E. K. Lee,² H. Lee,^{1,2} H. S. Lee,^{2,1,‡} H. Y. Lee,⁹ I. S. Lee,² J. Lee,² J. Y. Lee,⁴ M. H. Lee,^{2,1} S. H. Lee,^{1,2} S. H. Lee,¹³ Y. J. Lee,⁸ D. S. Leonard,² N. T. Luan,⁴ V. H. A. Machado,³ B. B. Manzato,³ R. H. Maruyama,¹⁴ S. L. Olsen,² H. K. Park,¹² H. S. Park,¹⁵ J. C. Park,¹⁶ J. S. Park,⁴ K. S. Park,² K. Park,² S. D. Park,⁴ R. L. C. Pitta,³ H. Prihtiadi,⁷ C. Rott,¹⁷ K. A. Shin,² D. F. F. S. Cavalcante,³ M. K. Son,¹⁶ N. J. C. Spooner,⁶ L. T. Truc,⁴ L. Yang,¹⁸ and G. H. Yu²

(COSINE-100 Collaboration)

¹*IBS School, University of Science and Technology (UST), Daejeon 34113, Republic of Korea*

²*Center for Underground Physics, Institute for Basic Science (IBS), Daejeon 34126, Republic of Korea*

³*Physics Institute, University of São Paulo, 05508-090, São Paulo, Brazil*

⁴*Department of Physics, Kyungpook National University, Daegu 41566, Republic of Korea*

⁵*Department of Physics and Astronomy, Seoul National University, Seoul 08826, Republic of Korea*

⁶*Department of Physics and Astronomy, University of Sheffield, Sheffield S3 7RH, United Kingdom*

⁷*Department of Physics, Universitas Negeri Malang, Malang 65145, Indonesia*

⁸*Department of Physics, Chung-Ang University, Seoul 06973, Republic of Korea*

⁹*Center for Exotic Nuclear Studies, Institute for Basic Science (IBS), Daejeon 34126, Republic of Korea*

¹⁰*Department of Science Education, Ewha Womans University, Seoul 03760, Republic of Korea*

¹¹*Department of Physics and Wisconsin IceCube Particle Astrophysics Center, University of Wisconsin-Madison, Madison, WI 53706, USA*

¹²*Department of Accelerator Science, Korea University, Sejong 30019, Republic of Korea*

¹³*Department of Physics, Jeju National University, Jeju 63243, Republic of Korea*

¹⁴*Department of Physics and Wright Laboratory, Yale University, New Haven, CT 06520, USA*

¹⁵*Korea Research Institute of Standards and Science, Daejeon 34113, Republic of Korea*

¹⁶*Department of Physics and Institute for Sciences of the Universe, Chungnam National University, Daejeon 34134, Republic of Korea*

¹⁷*Department of Physics and Astronomy, University of Utah, Salt Lake City, UT 84112, USA*

¹⁸*Department of Physics, University of California San Diego, La Jolla, CA 92093, USA*

We report new constraints on the spin-dependent scattering cross section between low-mass dark matter and protons using data collected by the COSINE-100 experiment. By implementing a specialized event selection process using a multi-layer perceptron and robust noise mitigation, this analysis pioneers a detection threshold of 3 and 4 isolated peaks, corresponding to the reconstructed photoelectrons, which is significantly lower than the 8 photoelectron threshold used in previous analyses. In this unstudied few-photoelectron regime, where PMT-induced noise and phosphorescence are prevalent, we utilize a phenomenological background model to search for the annual modulation signal expected from the Standard Halo Model. No statistically significant annual modulation is observed in our data. We derive new 90% confidence level upper limits for the spin-dependent DM-proton cross section, establishing the world's most stringent constraints in the 1.75–2.25 GeV/c² mass range. Furthermore, by incorporating the Migdal effect, we extend the experimental sensitivity to the sub-GeV/c² regime, setting world-leading limits in the 15–58 MeV/c² range. These results demonstrate the capability of NaI(Tl) target materials to probe previously unexplored regions of the dark matter parameter space.

Introduction.—The existence of Dark Matter (DM), constituting approximately 27% of the Universe's total energy density, is strongly supported by a wide range of astrophysical and cosmological observations [1–3]. Weakly Interacting Massive Particles (WIMPs) have long been considered among the most compelling candidates for DM [4–6]. Direct detection experiments aim to observe the elastic scattering of WIMPs off atomic nuclei, resulting in nuclear recoils [5–7]. Recently, increasing attention has focused on low-mass DM with masses below a few GeV/c², where the resulting small recoil en-

ergies requires the use of advanced detectors with energy thresholds reduced below 1 keV [8–11].

The search for such light DM candidates can be addressed by considering the Migdal effect [12–15]. This effect occurs when the inherent resilience of atomic electrons is insufficient to accommodate the sudden acceleration of a recoiling nucleus, leading to excitation or ionization. This process allows experiments to extend their sensitivity into the sub-GeV/c² mass range [16–19]. Recently, the Migdal effect has been observed in neutron-nucleus interactions with nuclear recoil energy

above 35 keV and electron energy of 5–10 keV [20], where the observed effect is consistent with theoretical predictions.

The COSINE-100 experiment [21, 22], utilizing NaI(Tl) scintillating crystals, offers a distinct advantage for probing spin-dependent (SD) DM-proton interactions due to the presence of ^{23}Na and ^{127}I isotopes, both of which being proton-odd nuclei. Furthermore, the relatively low atomic mass of sodium enhances sensitivity to low-mass dark matter compared to experiments employing heavier target materials. This intrinsic sensitivity, combined with the development of techniques to reach the few-photoelectron (PE) regime, allows us to effectively bridge the gap in sub-GeV/ c^2 dark matter searches.

In this Letter, we present the result of a search for low-mass DM using the COSINE-100 data. Crucially, we use a pioneering few-PE threshold, analyzing data at the 3 and 4 pulse peaks level. This threshold is significantly below the 8 PE threshold employed in previous COSINE-100 analyses [19, 23–25]. We exploit this low-threshold data to search for an annual modulation signal and set new constraints on the SD DM-proton cross section, including limits extended by the Migdal effect.

Experimental setup.—The COSINE-100 experiment situated at the Yangyang Underground Laboratory in South Korea was protected by an overburden of approximately 700 m of rock [26, 27]. The detector commenced data acquisition in October 2016 and operated until March 2023, totaling 6.4 years of exposure [25]. The primary detection mass consists of eight low-background NaI(Tl) scintillating crystals with a combined mass of 106 kg [21, 22]. Each crystal is coupled to two high-quantum-efficiency Hamamatsu R12669SEL 3-inch photomultiplier tubes (PMTs) at opposite ends.

To achieve a low-energy threshold, we require a minimum trigger condition: the detection of at least one PE in each of the two PMTs within a 200 ns coincidence time window [28]. This trigger condition efficiently acquires 3 and 4 pulse peaks events that are of interest in this analysis. To further reduce backgrounds, the crystal array is immersed in a 2,200 L liquid scintillator (LS) veto [29], and the entire assembly is shielded by a nested structure comprising thickness of 3 cm copper, 20 cm lead, and an outer 3 cm plastic scintillator panel array to veto cosmic muons [21].

This analysis focuses on single-hit events, as the low DM cross-section makes coincident interactions across multiple crystals highly improbable. The single-hit events are defined as energy depositions occurring in only one crystal, with no coincident signals observed in the other seven crystals or the veto detectors. Multiple-hit events are utilized to understand and characterize background characteristics. Due to high noise rate of crystal 1 and low light yields of crystals 5 and 8, we utilize only five crystals (crystals 2, 3, 4, 6, and 7), consistent with

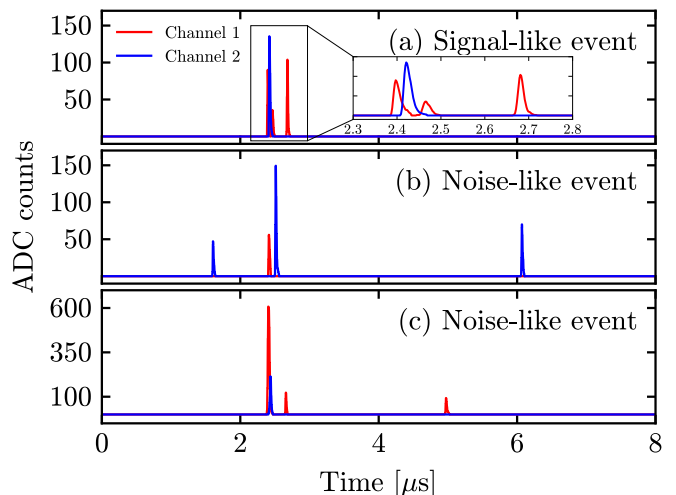


FIG. 1. Representative waveforms for NC-4 events in a NaI(Tl) crystal. (a) A signal-like event passing the MLP selection criteria, with clusters distributed within the characteristic 200 ns scintillation decay time. The inset provides a zoomed-in view of the 2.3–2.8 μs region, clearly illustrating the individual photon clusters within the pulse. (b) A noise-like event rejected by the MLP selection due to clusters distributed over a broader time interval, characteristic of phosphorescence. (c) A noise-like event induced by Cherenkov radiation in the PMT glass, characterized by an anomalous single-cluster profile, rejected by the cluster charge cut.

previous analyses [19, 25, 30]. To avoid short-lived cosmogenic contributions [24, 31], approximately 2.4-years of the initial operation period were excluded, leaving a relatively stable 4-year dataset for the analysis.

Event selection.—The exploration of low-mass DM requires pushing the detection threshold down to the few-PE level, which is substantially below previous COSINE-100 analysis thresholds. To target these few-PE energy depositions, we define the number of clusters (NCs) as the count of isolated, localized peaks in a waveform that exceed a pedestal-based threshold using the clustering algorithm described in Ref. [32] and exhibit a single PE-like profile as shown in Fig. 1.

To characterize signal behavior at this level, we utilize a detailed NaI(Tl) waveform simulation [33] that incorporates measured scintillation characteristics and single-PE pulse shapes. This simulation allows us to evaluate the detector’s trigger efficiency by applying the hardware requirements directly to the simulated events. We obtained a trigger efficiency of 62.5% and 81.0% for NC-3 and NC-4 events, respectively. The results confirm that events generated with a fixed number of PEs produce a reconstructed NC distribution centered around the input value, providing a reliable mapping between physical energy depositions and our observed NC counts.

A three-step event selection process was implemented to contend with the unique noise contributions in this unstudied region. First, a Deadtime cut was applied

to abate phosphorescence events—delayed light emissions following high-energy (HE) precedent events—that can mimic genuine low-energy signals [34]. This cut was optimized for two HE regions: 0.3 s for events between 1 MeV and 3.2 MeV, and 2.2 s for events above 3.2 MeV. This initial filter achieved a high signal retention of 97% while simultaneously reducing noise events by approximately 31.5% in NC-3 and 22.2% in NC-4.

Then, a complementary cluster charge cut was applied to remove abnormally large single clusters typically caused by Cherenkov radiation in the PMT glass. The cut boundary was defined conservatively to preserve a signal efficiency of approximately 97%, ensuring negligible impact on genuine low energy scintillation events. This cut reduces the noise level by approximately 10% in NC-3 and 15% in NC-4.

To achieve further separation between signal and noise, a machine learning technique using a multi-layer perceptron (MLP) in the ROOT TMVA toolkit [35, 36] was employed, similar to recent COSINE-100 analyses [19, 23, 24]. The MLP was trained separately for each crystal and NC count using kinematic variables such as the time difference between clusters and the charge asymmetry between the two PMTs. The signal dataset for training was derived from the aforementioned waveform simulations, while the noise dataset was constructed directly from the physics data.

The MLP training is designed to retain signal-like events, characterized by isolated clusters well-distributed within the 200 ns decay time of NaI(Tl), as illustrated in Fig. 1(a). Conversely, it is trained to reject noise-like events where clusters are distributed over much wider windows typically caused by phosphorescence, as shown in Fig. 1(b). Given the difficulty of perfect separation, we chose selection criteria resulting in a 50% signal efficiency, which provided an average noise rejection of approximately 91% for NC-3 and 97% for NC-4 events that already passed the Deadtime selection. Fig. 1(c) illustrates the noise-like events rejected by the preceding cluster charge cut, such as those induced by Cherenkov radiation.

Only single-hit events passing the Deadtime, cluster charge, and MLP cuts were used in the subsequent annual modulation search. After applying all selection criteria, stability of detector was monitored using the multiple-hit events sideband. Large rate fluctuations were observed in crystal 2 for initial four years of the data period. To maintain data integrity, this unstable period for crystal 2 was excluded from the analysis. Consequently, the final dataset utilized for the search consists of the latest stable 4-year period for crystal 3, 4, 6, and 7, and a 2-year period for crystal 2.

Annual modulation.—Following the rigorous event selection using Deadtime, cluster charge, and MLP cuts, the remaining dataset consists of a mixture of radioactive backgrounds and unexpected noise contributions from

PMT-induced events and phosphorescence, and the potential signal from DM interactions. Because a comprehensive physics-based background simulation is currently unfeasible for the few-PE region, we adopt a phenomenological approach to model the time-dependent background and search for a superimposed annual modulation signal. The time evolution of the event rate, $F(t; A)$, is modeled using a function that incorporates a constant baseline C , an exponential component to account for decaying background elements, and a sinusoidal function representing the DM-induced modulation:

$$F(t; A) = A \cos \left[\frac{2\pi}{T}(t - \phi) \right] + \exp(p_0 + p_1 t) + C, \quad (1)$$

where A is the modulation amplitude, p_0 and p_1 are the parameters for exponential background. Based on the Standard Halo Model (SHM) and Earth’s orbital dynamics, the period T is fixed to 365.25 days (1 year), and the phase ϕ is fixed to 152.5 days [37–39]. Simultaneous fits across the crystals are performed on 15-day time-binned data for the stable period. To rigorously evaluate the stability of the signal region, we utilize a sideband consisting of events neighboring the MLP selection region. This sideband includes events classified as noise by the 50% signal acceptance cut but contains an equivalent volume of data. According to waveform simulations, approximately 20% and 17% of genuine signal events for the NC-3 and NC-4 categories, respectively, are accepted into the noise-classified sideband region.

We observed that the NC-3 dataset exhibited significant fluctuations, resulting in a reduced χ^2 greater than unity. To account for this instability in the signal region, we derived a scale factor for each crystal, specifically calculated to bring the reduced χ^2 of the sideband to unity. This value is then assigned as a relative crystal-specific systematic uncertainty (δu_i), derived from the sideband stability analysis. The χ^2 function is defined as:

$$\chi^2 = \sum_i^{N_{\text{crystal}}} \sum_j^{N_{\text{time}}} \frac{[M_{ij} - F_i(t_j; A)]^2}{M_{ij} + \delta u_i^2 M_{ij}^2}, \quad (2)$$

where M_{ij} is the observed count in time bin j of crystal i and $F_i(t_j; A)$ is the model in Eq. (1). The systematic uncertainties are treated as fully uncorrelated between bins.

Fig. 2 presents the results of simultaneous fits performed across the five crystals, conducted separately for the NC-3 (left) and NC-4 (right) datasets. Goodness-of-fit is quantified by χ^2/NDF (number of degrees of freedom), with the observed modulation amplitude A amplified by 100 times for visibility, as indicated in each panel. Given the sufficiently large NDF, reduced χ^2 values close to unity are observed, proving statistically consistent fits.

No statistically significant modulation was observed in either case. Identical fits performed on multiple-hit

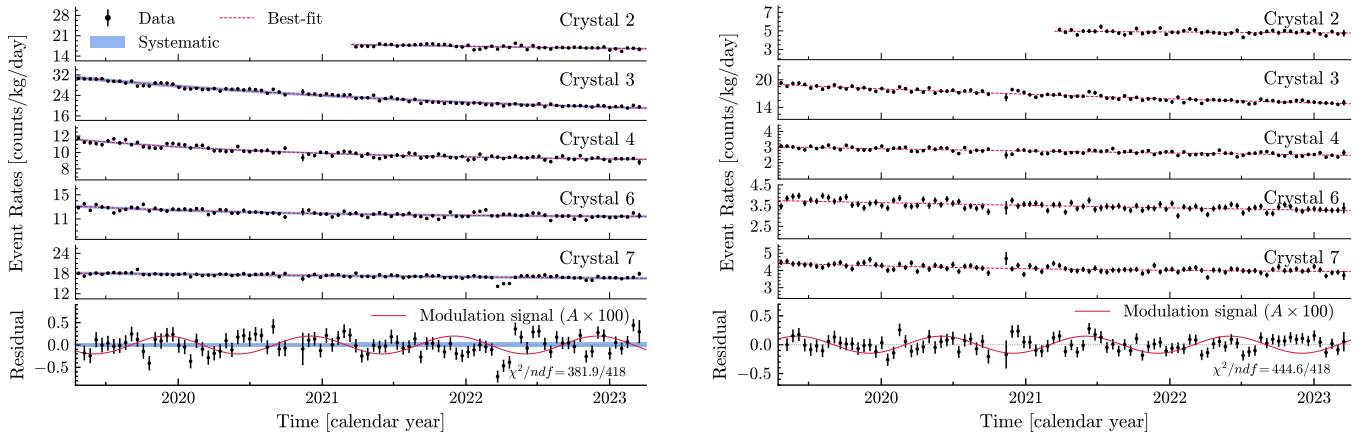


FIG. 2. Event rates as a function of time for the five NaI(Tl) crystals used in the analysis, overlaid with the best-fit annual modulation model for single-hit events. Data are grouped in 15-day bins, and the fits are performed simultaneously across all crystals with a fixed phase of 152.5 days and a shared modulation amplitude A . The bottom panels show the residuals from the fits. (Left) The NC-3 dataset is shown with the blue shaded bands representing the systematic uncertainties (δu_i). (Right) The NC-4 dataset is shown.

Number of clusters [NCs]	Amplitude (A) [counts/kg/day]	
	Single-hit	Multiple-hit
3	-0.002 ± 0.026	0.002 ± 0.007
4	0.001 ± 0.011	0.002 ± 0.003

TABLE I. Best-fit annual modulation amplitudes (A) obtained from the simultaneous fit of five crystals, performed separately for the NC-3 and NC-4 pulse cluster bins. Results for both single-hit (signal) and multiple-hit (background control) events are consistent with the null hypothesis, showing no statistically significant modulation.

events consistently showed no modulation, as summarized in Table I. In the absence of a modulated signal, these results are used to establish new constraints on the SD DM–proton cross section.

Dark matter limits.—To translate the null result from the annual modulation search into constraints on DM cross sections, we calculate the expected signal based on the SHM. The differential DM–nucleon induced recoil rate is calculated using the DMDD package [40–42]. The expected modulation amplitude, $A'(\sigma_{\text{DM}})$, for each DM model is derived from the difference in recoil rates between the maximum and minimum Earth speeds ($v_{\text{max}} \approx 247$ km/s and $v_{\text{min}} \approx 217$ km/s), reflecting the annual velocity variation of DM interactions [6, 7, 37, 39]. These physical spectra are converted to observable NC distributions through a comprehensive detector response model, applying measured light yields [21] and quenching factors [43], processed through detailed waveform simulations [33].

Because the expected DM signal provides a linked constraint across both the NC-3 and NC-4 datasets, we reconstruct the χ^2 function to simultaneously fit all se-

lected crystals and NC bins:

$$\chi^2(\sigma_{\text{DM}}) = \sum_i^{\text{NC}} \sum_j^{N_{\text{crystal}}} \sum_k^{N_{\text{time}}} \frac{[M_{ijk} - F_{ij}(t_k; A')]^2}{M_{ijk} + \delta u_{ij}^2 M_{ijk}^2} + \left(\frac{\alpha_{ij}}{\delta c_{ij}} \right)^2, \quad (3)$$

where M_{ijk} is the observed count in time bin k for crystal j and NC bin i , and $F_{ij}(t_k; A')$ is the DM-induced modulation model as defined in Eq. (1), where the modulation amplitude A is replaced by the expected amplitude A' . In this framework, A' is directly tied to the DM cross-section:

$$A'(\sigma_{\text{DM}}) = (1 + \alpha_{ij}) f_{ij}(m_{\text{DM}}) \sigma_{\text{DM}}, \quad (4)$$

where $f_{ij}(m_{\text{DM}})$ is a conversion factor from the cross-section σ_{DM} to event rates (counts/kg/day), and α_{ij} is a nuisance parameter accounting for light yield errors with a relative uncertainty δc_{ij} . Upper limits are established at a 90% confidence level (C.L.) based on maximum likelihood estimation using Eq. (3). A Probability Density Function (PDF) for each mass is defined as:

$$\text{PDF} = C \exp\left(-\frac{\Delta\chi^2}{2}\right), \quad (5)$$

where C is a normalization factor ensuring the PDF integrates to unity over the physical region ($\sigma_{\text{DM}} \geq 0$), and $\Delta\chi^2 = \chi^2(\sigma_{\text{DM}}) - \chi_{\text{min}}^2$. In this analysis, χ_{min}^2 denotes the minimum value of $\chi^2(\sigma_{\text{DM}})$.

As shown in Fig. 3(Top), we set new constraints on the SD DM–proton cross section in the 1.2–3.0 GeV/ c^2 mass region. Notably, this work probes a previously unexplored parameter space between 1.75 and 2.25 GeV/ c^2 that has not been constrained by other experiments [10, 16, 19, 44–47]. Furthermore, the inclusion of the Migdal effect extends our reach to masses as low as 15 MeV/ c^2 ,

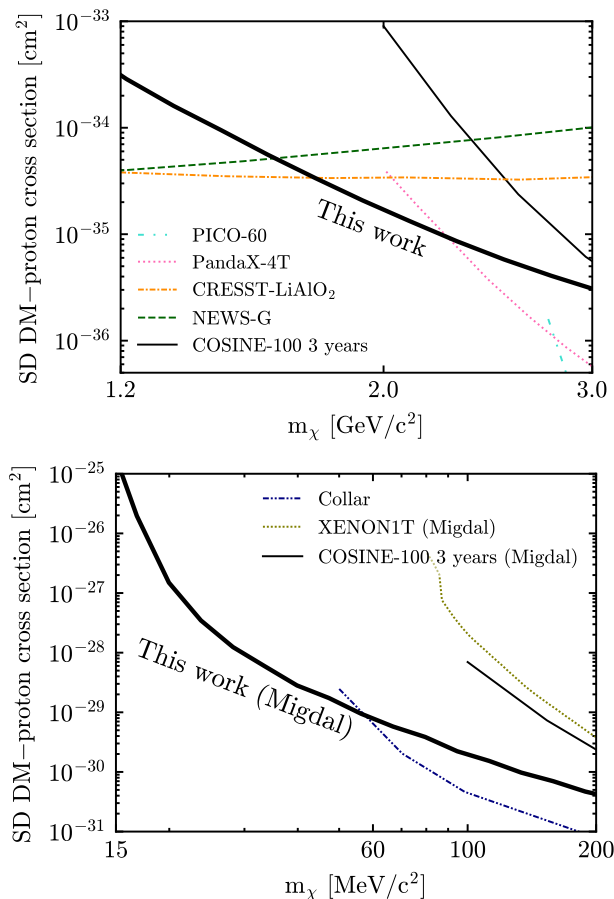


FIG. 3. The derived 90% C.L. upper limits on the SD DM-proton cross section as a function of DM mass m_χ . The thick solid line represents the result of this work. (Top) Constraints in the 1.2–3.0 GeV/ c^2 mass region for standard SD nuclear recoils. Our result provides new constraints in the 1.75–2.25 GeV/ c^2 range, a region not previously explored by the compared experiments: PICO [44], PandaX-4T [45], CRESST-LiAlO₂ [46], NEWS-G [10], and the recent COSINE-100 3-year data result [19]. (Bottom) Extended sensitivity in the 15–200 MeV/ c^2 region enabled by the Migdal effect. Our results establish stringent new limits in the 15–58 MeV/ c^2 range, significantly extending the reach beyond the 100 MeV/ c^2 limit achieved in previous COSINE-100 3-year data result [19]. This work surpasses the previous experimental reach of Collar [47] and XENON1T [16].

as illustrated in Fig. 3(Bottom). While our previous analysis (COSINE-100 3 years) using an 8 PE threshold reached limits down to 100 MeV/ c^2 [19], this NC-3 and NC-4 threshold analysis establishes stringent new limits between 15 and 58 MeV/ c^2 . These results demonstrate the capability of NaI(Tl) target materials to probe previously unexplored regions of the dark matter parameter space.

Conclusion.—We have established a new detection threshold for NaI(Tl) at the 3-PE level. This low-threshold analysis successfully isolates signals from PMT

noise and phosphorescence, allowing us to probe unexplored parameter spaces. We established new 90% C.L. constraints for SD DM-proton cross section in the 1.75–2.25 GeV/ c^2 range and, via the Migdal effect, in the 15–58 MeV/ c^2 mass range. This provides a critical foundation for COSINE-100U [48] at Yemilab, where higher light yields will further enhance sensitivity to light dark matter.

We thank the Korea Hydro and Nuclear Power (KHNP) Company for providing underground laboratory space at Yangyang and the IBS Research Solution Center (RSC) for providing high performance computing resources. This work is supported by: the Institute for Basic Science (IBS) under project code IBS-R016-A1, NRF-2021R1A2C3010989, NRF-2021R1A2C1013761, RS-2024-00356960, RS-2025-25442707 and RS-2025-16064659, Republic of Korea; NSF Grants No. PHY-1913742, United States; STFC Grant ST/N000277/1 and ST/K001337/1, United Kingdom; Grant No. 2021/06743-1, 2022/12002-7, 2022/13293-5 and 2025/01639-2 FAPESP, CAPES Finance Code 001, CNPq 304658/2023-5, Brazil; UM Internal Grant non-APBN 2025, Indonesia.

* wonkkim30@gmail.com

† yjkophys@jejunu.ac.kr

‡ hyunsulee@ibs.re.kr

- [1] M. Persic, P. Salucci, and F. Stel, The Universal rotation curve of spiral galaxies: 1. The Dark matter connection, *Mon. Not. Roy. Astron. Soc.* **281**, 27 (1996).
- [2] N. Aghanim *et al.*, Planck 2018 results. VI. Cosmological parameters, *Astron. Astrophys.* **641**, A6 (2020).
- [3] D. Scognamiglio *et al.*, An ultra-high-resolution map of (dark) matter, *Nat. Astron.* [10.1038/s41550-025-02763-9](https://doi.org/10.1038/s41550-025-02763-9) (2026).
- [4] B. W. Lee and S. Weinberg, Cosmological Lower Bound on Heavy-Neutrino Masses, *Phys. Rev. Lett.* **39**, 165 (1977).
- [5] T. M. Undagoitia and L. Rauch, Dark matter direct-detection experiments, *J. Phys. G* **43**, 013001 (2016).
- [6] M. Schumann, Direct Detection of WIMP Dark Matter: Concepts and Status, *J. Phys. G* **46**, 103003 (2019).
- [7] M. W. Goodman and E. Witten, Detectability of Certain Dark Matter Candidates, *Phys. Rev. D* **31**, 3059 (1985).
- [8] R. Agnese *et al.* (SuperCDMS Collaboration), Low-mass dark matter search with CDMSlite, *Phys. Rev. D* **97**, 022002 (2018).
- [9] A. H. Abdelhameed *et al.* (CRESST Collaboration), First results from the CRESST-III low-mass dark matter program, *Phys. Rev. D* **100**, 102002 (2019).
- [10] M. M. Arora *et al.* (NEWS-G Collaboration), Search for Light Dark Matter with NEWS-G at the Laboratoire Souterrain de Modane Using a Methane Target, *Phys. Rev. Lett.* **134**, 141002 (2025).
- [11] P. Adari *et al.* (SENSEI Collaboration), First Direct-Detection Results on Sub-GeV Dark Matter Using the

- SENSEI Detector at SNOLAB, *Phys. Rev. Lett.* **134**, 011804 (2025).
- [12] A. Migdal, Ionizatsiya atomov pri yadernykh reaktivnykh, *Sov. Phys. JETP* **9** (1939).
- [13] A. Migdal, Ionizatsiya atomov v α -i β -raspade, *Zh. Eksp. Teor. Fiz.* **11**, 207 (1941).
- [14] M. Ibe, W. Nakano, Y. Shoji, and K. Suzuki, Migdal effect in dark matter direct detection experiments, *JHEP* **2018** (3), 194.
- [15] J. D. Vergados, Searching for light WIMPs via their interaction with electrons, *J. Phys. G* **47**, 095007 (2020).
- [16] E. Aprile *et al.* (XENON Collaboration), Search for Light Dark Matter Interactions Enhanced by the Migdal Effect or Bremsstrahlung in XENON1T, *Phys. Rev. Lett.* **123**, 241803 (2019).
- [17] G. Adhikari *et al.* (COSINE-100 Collaboration), Searching for low-mass dark matter via the Migdal effect in COSINE-100, *Phys. Rev. D* **105**, 042006 (2022).
- [18] P. Agnes *et al.* (DarkSide Collaboration), Search for Dark-Matter–Nucleon Interactions via Migdal Effect with DarkSide-50, *Phys. Rev. Lett.* **130**, 101001 (2023).
- [19] G. H. Yu *et al.* (COSINE-100 Collaboration), Limits on WIMP dark matter with NaI(Tl) crystals in three years of COSINE-100 data, *Phys. Rev. Lett.* **135**, 231001 (2025).
- [20] D. Yi *et al.*, Direct observation of the Migdal effect induced by neutron bombardment, *Nature* **649**, 580 (2026).
- [21] G. Adhikari *et al.* (COSINE-100 Collaboration), Initial Performance of the COSINE-100 Experiment, *Eur. Phys. J. C* **78**, 107 (2018).
- [22] P. Adhikari *et al.* (COSINE-100 Collaboration), Background model for the NaI(Tl) crystals in COSINE-100, *Eur. Phys. J. C* **78**, 490 (2018).
- [23] G. H. Yu *et al.* (COSINE-100 Collaboration), Lowering threshold of NaI(Tl) scintillator to 0.7 keV in the COSINE-100 experiment, *JINST* **19** (12), P12013, [arXiv:2408.14688 \[hep-ex\]](https://arxiv.org/abs/2408.14688).
- [24] G. H. Yu *et al.* (COSINE-100 Collaboration), Improved background modeling for dark matter search with COSINE-100, *Eur. Phys. J. C* **85**, 32 (2025).
- [25] S. M. Lee *et al.* (COSINE-100 Collaboration), COSINE-100 full dataset challenges the annual modulation signal of DAMA/LIBRA, *Sci. Adv.* **11**, eadv650 (2025).
- [26] H. Prihtiadi *et al.* (COSINE-100 Collaboration), Muon detector for the COSINE-100 experiment, *JINST* **13** (02), T02007.
- [27] H. Prihtiadi *et al.* (COSINE-100 Collaboration), Measurement of the cosmic muon annual and diurnal flux variation with the COSINE-100 detector, *JCAP* **02**, 013.
- [28] G. Adhikari *et al.* (COSINE-100 Collaboration), The COSINE-100 Data Acquisition System, *JINST* **13** (09), P09006.
- [29] G. Adhikari *et al.* (COSINE-100 Collaboration), The COSINE-100 Liquid Scintillator Veto System, *Nucl. Instrum. Methods Phys. Res. A* **1006**, 165431 (2020).
- [30] G. Adhikari *et al.* (COSINE-100 Collaboration), An experiment to search for dark-matter interactions using sodium iodide detectors, *Nature* **564**, 83 (2018).
- [31] E. Barbosa de Souza *et al.* (COSINE-100 Collaboration), Study of cosmogenic radionuclides in the COSINE-100 NaI(Tl) detectors, *Astropart. Phys.* **115**, 102390 (2020).
- [32] H. S. Lee *et al.* (KIMS Collaboration), First limit on WIMP cross section with low background CsI(Tl) crystal detector, *Phys. Lett. B* **633**, 201 (2006).
- [33] J. J. Choi *et al.*, Waveform simulation for scintillation characteristics of NaI(Tl) crystal, *Nucl. Instrum. Meth. A* **1065**, 169489 (2024).
- [34] J. Cherwinka *et al.* (DM-Ice Collaboration), Measurement of Muon Annual Modulation and Muon-Induced Phosphorescence in NaI(Tl) Crystals with DM-Ice17, *Phys. Rev. D* **93**, 042001 (2016).
- [35] R. Brun and F. Rademakers, ROOT: An object oriented data analysis framework, *New computing techniques in physics research V. Proceedings, 5th International Workshop, AIHENP '96, Lausanne, Switzerland, September 2-6, 1996* **A389**, 81 (1997).
- [36] A. Hoecker, P. Speckmayer, J. Stelzer, J. Therhaag, E. von Toerne, H. Voss, M. Backes, T. Carli, O. Cohen, A. Christov, D. Dannheim, K. Danielowski, S. Henrot-Versille, M. Jachowski, K. Kraszewski, A. K. Jr, M. Kruk, Y. Mahalalel, R. Ospanov, X. Prudent, A. Robert, D. Schouten, F. Tegenfeldt, A. Voigt, K. Voss, M. Wolter, and A. Zemla, *TMVA - Toolkit for Multivariate Data Analysis* (2009), [arXiv:physics/0703039](https://arxiv.org/abs/physics/0703039).
- [37] J. Lewin and P. Smith, Review of mathematics, numerical factors, and corrections for dark matter experiments based on elastic nuclear recoil, *Astropart. Phys.* **6**, 87 (1996).
- [38] K. Freese, J. A. Frieman, and A. Gould, Signal Modulation in Cold Dark Matter Detection, *Phys. Rev. D* **37**, 3388 (1988).
- [39] K. Freese, M. Lisanti, and C. Savage, Colloquium: Annual modulation of dark matter, *Rev. Mod. Phys.* **85**, 1561 (2013).
- [40] V. Gluscevic and S. D. McDermott, dmdd: Dark matter direct detection, *Astrophysics Source Code Library*, record ascl:1506.002 (2015).
- [41] V. Gluscevic, M. I. Gresham, S. D. McDermott, A. H. G. Peter, and K. M. Zurek, Identifying the Theory of Dark Matter with Direct Detection, *JCAP* **1512** (12), 057.
- [42] N. Anand, A. L. Fitzpatrick, and W. C. Haxton, Weakly interacting massive particle-nucleus elastic scattering response, *Phys. Rev. C* **89**, 065501 (2014).
- [43] S. H. Lee *et al.*, Measurements of low-energy nuclear recoil quenching factors for Na and I recoils in the NaI(Tl) scintillator, *Phys. Rev. C* **110**, 014614 (2024).
- [44] C. Amole *et al.* (PICO Collaboration), Dark matter search results from the complete exposure of the PICO-60 c₃f₈ bubble chamber, *Phys. Rev. D* **100**, 022001 (2019).
- [45] M. Zhang *et al.* (PandaX Collaboration), Search for Light Dark Matter with 259-day data in PandaX-4T, *Phys. Rev. Lett.* **135**, 211001 (2025).
- [46] G. Angloher *et al.* (CRESST Collaboration), Testing spin-dependent dark matter interactions with lithium aluminate targets in CRESST-III, *Phys. Rev. D* **106**, 092008 (2022).
- [47] J. I. Collar, Search for a nonrelativistic component in the spectrum of cosmic rays at Earth, *Phys. Rev. D* **98**, 023005 (2018).
- [48] D. Lee *et al.* (COSINE-100 Collaboration), Upgrading the COSINE-100 experiment for enhanced sensitivity to low-mass dark matter detection, *Commun. Phys.* **8**, 135 (2025).